Resolution improvement in laser diode-based pump–probe microscopy with an annular pupil filter

Jun Miyazaki,[1,2] Koshi Kawasumi,[1] and Takayoshi Kobayashi[1,2,3,4,*]

[1]*Advanced Ultrafast Laser Research Center, The University of Electro-Communications, 1-5-1 Chofugaoka, Chofu, Tokyo 182-8585, Japan*

[2]*JST, CREST, K' Gobancho, 7, Gobancho, Chiyoda-ku, Tokyo 102-0076, Japan*

[3]*Department of Electrophysics, National Chiao-Tung University, Hsinchu 300, Taiwan*

[4]*Institute of Laser Engineering, Osaka University, 2-6 Yamada-oka, Suita, Osaka 565-0971, Japan*

**Corresponding author: kobayashi@ils.uec.ac.jp*

Received April 2, 2014; accepted May 29, 2014;
posted June 4, 2014 (Doc. ID 209420); published July 11, 2014

We experimentally demonstrate the use of annular beams to improve lateral resolution in laser-diode-based pump–probe microscopy. We found that the width of the point-spreading function in the case of the annular pump–probe beams is 162 nm, which is 30% smaller than that of the circular beams (232 nm). Furthermore, side lobes were efficiently suppressed at the focal plane since the pump–probe signal is proportional to the product of the two beam intensities. This scheme is demonstrated for the photothermal signal of nonfluorescent gold nanoparticles and the stimulated emission signal of fluorescence beads. © 2014 Optical Society of America

OCIS codes: (180.0180) Microscopy; (140.2020) Diode lasers; (100.6640) Superresolution.
http://dx.doi.org/10.1364/OL.39.004219

Pump–probe techniques have been widely used in the field of optical microscopy for imaging of fluorophores that have short-lived excited states [1–3], label-free biological imaging such as with red blood cells [4,5], analysis of melamine pigments and melanoma diagnosis [6–8], and nondestructive 3D imaging of a 14th-century painting [9]. Recent development of pump–probe microscopy has been carried out typically using high-intensity femtosecond pulse trains with high repetition rates and high-frequency lock-in detection schemes to avoid laser-intensity fluctuation, which is larger at lower frequencies. More recently, we implemented pump–probe microscopy using intensity-modulated laser diodes in which shot-noise-limited sensitivity was achieved using balanced detection scheme [10]. By using our technique, biological imaging of mouse T cells and axons of neurons in the cerebral cortex was demonstrated. The cost of LD was lower than in the Ti:sapphire-laser-based system. Furthermore, LD is maintenance free and power consumption and space occupied by the instruments were reduced in comparison with the mode-locked-laser-based system.

The spatial resolution obtained using a pump–probe microscope is better than that using a conventional fluorescence intensity microscope because the pump–probe signal is intrinsically a third-order process based on the nonlinear interaction between the two laser beams and the sample. We showed that the point spreading function (PSF) in pump–probe microscopy is 23% (43%) smaller than the diffraction limited spot size of the pump (probe) beam [10]. It is important to note that sub-diffraction resolution can be achieved even for weak fluorescent species; it is usually more photostable and hence less toxic than fluorescent molecules due to fast relaxation to the ground state resulting in the intersystem crossing to triplet state and chemical reaction channels. Therefore it is potentially useful as probe material in biological imaging.

In this study, we demonstrate the use of annular beams in our pump–probe microscopy to improve spatial resolution in the focal plane. A focusing annular beam is known to exhibit a sharpened main peak with large side lobes in the focal plane [11]. The application of the annular beam has attracted much attention in the field of scanning microscopy over the past decades [12–21]. Several theoretical and numerical studies have suggested that it is possible to reduce the undesired side lobes and improve lateral resolution in nonlinear imaging, such as two-photon excitation (TPE) fluorescence microscopy, because of the square dependence of the intensity [12–14]. Recently, Serrels *et al.* experimentally demonstrated this lateral resolution enhancement in the TPE-induced current microscopic imaging of a silicon integrated circuit [15].

However, in TPE microscopy, near-infrared femtosecond pulses are usually employed for the light source since the photon energy should be half of the electronic excitation energy. This inherently limits the spatial resolution. In contrast, in the pump–probe measurement proposed here, a single pump photon can promote a molecule to an allowed electronic excited state, which in turn induces changes in probe transmissivity via excited-state absorption, ground-state absorption bleaching, and stimulated emission. Thus it is possible to select short wavelengths of visible light. Furthermore, in recent years, major advances have been made in high-power visible LDs, especially in blue-to-green-emitting InGaN-based LD [22,23]. Therefore, LD-based pump–probe microscopy with annular beams can substantially impact resolution enhancement.

We consider an annular beam of outer and inner diameters of D and εD, respectively, is focused at a distance f from aperture plane as shown in Fig 1(a). From the scalar diffraction theory, the intensity distribution of the annular beam in the focal plane is given by [11]

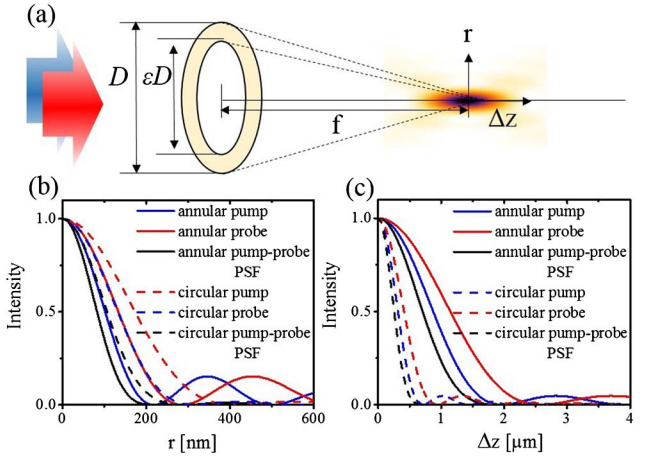

Fig. 1. Schematic of a focusing annular beam. (a) Geometry of an annular pump and probe beams with outer and inner diameters of D and εD, respectively. The beams are focusing at a distance f. (b), (c) Intensity profiles and the point spreading functions (PSFs) of the pump–probe signal in the focal plane (b) and in the axial direction (c) for the annular (solid lines) and circular (dashed lines) beams.

$$I_f(r) = (1-\varepsilon^2)^{-1}\{[I_c(\rho)]^{1/2} - \varepsilon^2[I_c(\varepsilon\rho)]^{1/2}\}^2, \quad (1)$$

where

$$I_c(r) = [2J_1(\pi\rho)/\pi\rho]^2 \quad (2)$$

represents the intensity radial distribution for the circular beam ($\varepsilon = 0$); $\rho = 2(\mathrm{NA})r/\lambda$ with $\mathrm{NA} = nD/f$ the numerical aperture of the focusing lens; n is the refractive index of the sample medium and we assume $n = 1$; r is the radial distance; and λ is the wavelength of the incident beam. Figure 1(b) shows I_f for pump and probe beams and their product (pump–probe PSF) for the annular and circular beams. We set an excitation wavelength of, nm and a probing wavelength of 640 nm. We also chose $\mathrm{NA} = 0.95$ and $\varepsilon = 0.8$. Note that I_f exhibits a sharp peak but is accompanied by large side lobes that compromise the resolution enhancement in conventional fluorescence microscopy [18]. The ratio of the first side lobe level to the main peak level (SLR) is 15%. However, the side lobes for pump–probe PSF are much reduced because of square dependence on the intensity as in the case of TPE fluorescence microscopy. The SLR for the pump–probe PSF is about 1%. It is important to note that the peak position of the first side lobe for the probe beam is shifted from that for pump beam by about 110 nm since the peak position is dependent on the wavelength. In the case of the present parameter set, SLR for the pump–probe PSF is about half of that for TPE-PSF (or for the pump–probe PSF with the same wavelengths). The FWHM of the pump–probe PSF for the annular beams is 164 nm, which is about 23% smaller than that for the circular beams of 212 nm.

We next calculated the PSF in the axial direction. The intensity distribution of the focusing annual beam along the optical axis in the limit of large Fresnel number ($D^2/(4\lambda f) \gg 1$) is given by

$$I_A(z) = (1-\varepsilon^2)(\sin W/W)^2, \quad (3)$$

where

$$W = \frac{\pi}{\lambda}(1-\varepsilon^2)\left(n - \sqrt{n - \mathrm{NA}^2}\right)\Delta z, \quad (4)$$

and Δz is the distance from the focal plane. The SLR in the intensity distributions of the pump and probe beams are 5%, while that of pump–probe PSF is reduced to be 0.1%. The FWHM of the pump–probe PSF for the annular beams is 1.4 μm, which is 2.8 times larger than that for the circular beams of 508 nm.

The effect of the annular beams on the spatial resolution is evaluated experimentally in our pump–probe microscopy system, which uses intensity modulated laser diodes (LDs) and a balance detector as illustrated in Fig. 2. We used a 488 nm LD for the pump, and a 640 nm LD for the probe beam. Each beam was collimated through a spatial filter, and two beams were combined using dichroic mirrors. The probe- and pump-beam intensities were set to frequencies of ω_1 and ω_2, respectively. A beat signal at $|\omega_1 - \omega_2|$ is generated by the bilinear interaction of the pump field and the probe field in the sample. A lock-in amplifier was referenced to the beat frequency. In this study, ω_1 and ω_2 were typically set at 1.000 and 1.015 MHz, respectively. To cancel the intensity fluctuation of the probe laser, we split the probe beam into two and directed the two resulting beams to an auto-balanced photodetector (Newfocus, Nirvana). This auto-balance detector serves to cancel both the laser noise and the intensity imbalance due to refractive-index variations during the sample scanning. We confirmed that when the probe beam power incident on the photodiode was above ~10 μW, the signal-to-noise ratio was mainly limited by shot noise. The pump and probe beams were linearly (vertically) polarized. A polarizing beam splitter was used to direct the combined beam to the objective lens (Olympus, UPLSAPO 40X2) with numerical NA of 0.95. The beam size was adjusted to fill the back aperture of the objective lens. The sample position was raster-scanned using a three-axis positioning stage driven by piezo actuators (Thorlabs, MAX311D). A 1.4-NA oil immersion condenser (Olympus, U-AAC) was used to collect the transmitted light. A narrow-band filter matching the laser line was placed in front of the detector to filter out both the excitation beam and the fluorescence

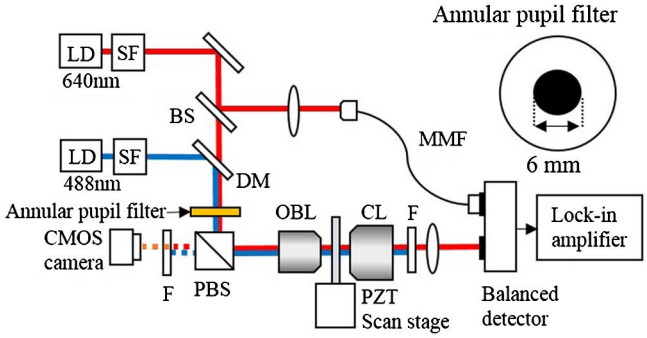

Fig. 2. Experimental setup of pump–probe microscopy using laser diodes. LD, laser diode; SF, spatial filter; DM, dichroic mirror; BS, beam splitter; ND, neutral density filter; PBS, polarization beam splitter; OBL, objective lens; CL, condenser lens; F, band pass filter; MMF, multimode fiber.

from the sample, so that only the probe beam was detected. A CMOS camera was used to check the sample position.

We made an annular pupil filter in such a way that a circular aluminum film with a diameter of 6 mm was prepared using a hole puncher, and then the film was attached to an optical flat. This filter was placed before the objective lens. The position of the annular pupil filter with respect to the optical axis was adjusted so that the transmitted beam formed a symmetric annular beam of 1.2 mm width.

We examined the spatial resolution by measuring the photothermal signal from 20 nm gold nanoparticles dispersed in a polyvinyl alcohol (PVA) film on a glass slide. The wavelength of the pump beam overlapped the absorption spectrum of the gold nanoparticles due to the plasmon resonance peak at 524 nm. In this case, pump light induces a temperature increase around a heated nanoparticle, which results in the local refractive index change. It then causes deflection of the probe beam, explained by an analogy to Rutherford scattering, and thus induces changes in the transmissivity [24]. The pump and probe powers incident on the sample were 0.7 and 0.3 mW, respectively. The typical time constant of the lock-in amplifier was 0.5 ms and the pixel dwell time was 1 ms. The sample plate was scanned in the focal plane [Fig. 3] and the optical axis plane [Fig. 4]. In the focal plane, fitting of a single particle with the Gaussian gives the full width at half-maximum (FWHM) values of 162 ± 4 nm and 196 ± 6 nm in the horizontal and vertical directions, respectively. We note that the intensity profile exhibits only a single peak and little or no side lobes are observed. Since the thickness of the PVA film is about 20 μm, gold nanoparticles are distributed in both the focal and axial planes. This leads to the intensity distribution in the xy image. Spatial resolution in the transverse

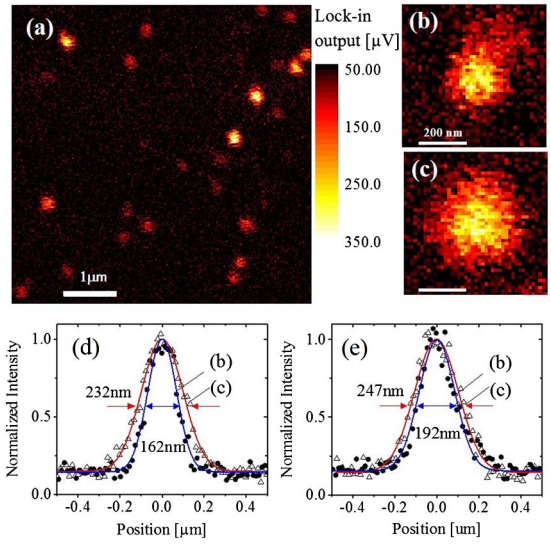

Fig. 3. Evaluation of lateral resolution in pump–probe microscopy. (a) pump–probe image (photothermal) of 20 nm gold nanoparticles dispersed on a glass slide for the annular beam. Number of pixels: 300×300. (b), (c) Single particle images for the annular (b) and circular (c) beams, respectively. Their intensity profiles in the horizontal and vertical directions are shown in (d) and (e), respectively.

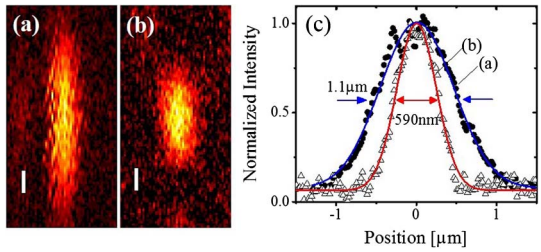

Fig. 4. Evaluation of axial resolution for the (a) annular and (b) circular beams. Scale bars indicate 200 nm. (c) Intensity distributions in the axial direction for (a) and (b).

direction is slightly better than that in the vertical direction because incident beams are linearly polarized in the vertical direction. We also measured the photothermal image of the gold nanoparticles in the case of the circular beams and found that the FWHM values were 232 ± 3 nm and 245 ± 7 nm in the horizontal and vertical directions, respectively. This result clearly demonstrates that our simple annual pupil filter is useful in improving the spatial resolution in the lateral direction. In contrast, the focal depth increases by about two for the annular beams as shown in Fig. 4. The axial FWHMs of gold nanoparticles were 1.1 ± 0.01 μm and 590 ± 9 nm for the annular and circular beams, respectively. This trend agrees with the results of the theoretical calculation shown in Fig. 1(c).

We confirm the effect of the annular beams in pump–probe microscopy on a fluorescent sample. Figure 5 shows the pump–probe image of 1 μm Nile red fluorescence beads for the (a) annular and (b) circular beams. The fluorescence beads are dispersed in PVA film between cover slips. The fluorescence had a peak around 600 nm and the probe beam wavelength overlaps the fluorescence spectrum at the long-wavelength edge as shown in Fig. 5(c). In this case, the stimulated emission may mainly contribute to the measured lock-in signal. Figure 5(d) shows the intensity profile along the broken lines. We found that the edge becomes sharper for the

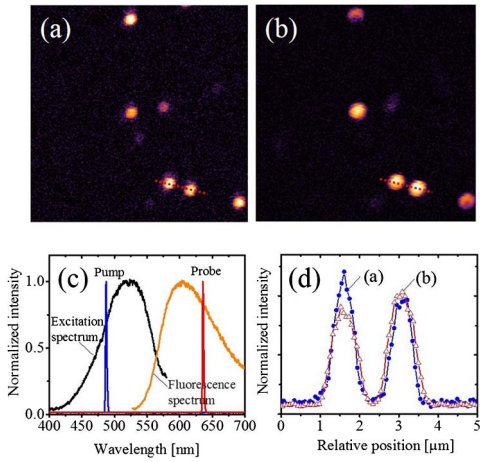

Fig. 5. Pump–probe (stimulated emission) image of 1 μm Nile red fluorescence beads for the (a) annular and (b) circular beams. The size of the field of view is 14.2×14.2 μm. (c) Excitation and fluorescence spectrum of Nile red fluorescence beads. The pump and probe light spectra are also shown. (d) Intensity profiles along the broken lines in (a) and (b).

annular beams. These results indicate that the annular beams are efficiently used to improve the lateral resolution for both fluorescence and nonfluorescence samples.

The annular pupil filter used in our experiment serves to increase the lateral resolution, but it also has some drawbacks. The light intensity decreases to 20% after passing through the filter in our setup. In pump–probe measurement, ultimate sensitivity would be achieved under the condition of saturated excitation. To induce saturation, pump-beam power should be above 1 mW, assuming the absorption cross section of 10^{-16} cm^2 and the excited state lifetime of 3 ns. One of the possible solutions to increase the beam intensity is to employ a phase plate with an apodization mask or an axicon lens to form annular beams [16,25]. Furthermore, the annual pupil filter elongates FWHM in the axial direction as shown in Fig. 4. This becomes a drawback when the structures in the axial direction need to be resolved, although the annular beam can be utilized to achieve depth imaging in conjugation with an orthogonal detection system [21]. It may be useful to introduce a central and peripheral annulus filter, which reduces deterioration in the axial resolution while keeping sub-diffraction resolution in the focal plane.

In conclusion, we have experimentally demonstrated the use of the annular pupil filter to improve the lateral resolution in pump–probe microscopy. The lateral resolution for the annular beams is 162 nm in FWHM, which is nearly half of the calculated focal spot size of the probe beam, $0.51\lambda/\mathrm{NA} = 340$ nm, and 30% smaller than that of the pump–probe PSF for circular beams (232 nm). The present scheme will allow us to resolve fine structures and to carry out functional analysis of biological tissues and nanomaterials.

This study was financially supported by a Grant-in-Aid for Scientific Research (No. 24740261) received from the Japan Society for the Promotion of Science and a joint research project at the Institute of Laser Engineering, Osaka University, under contract number B1-27.

References

1. W. Min, S. Lu, S. Chong, R. Roy, G. R. Holtom, and X. S. Xie, Nature **461**, 1105 (2009).
2. S. S. Chong, W. Min, and X. S. Xie, J. Phys. Chem. Lett. **1**, 3316 (2010).
3. L. Tong, Y. Liu, B. D. Dolash, Y. Jung, M. N. Slipchenko, D. E. Bergstrom, and J. X. Cheng, Nat. Nanotechnol. **7**, 56 (2012).
4. D. Fu, T. Ye, T. E. Matthews, B. J. Chen, G. Yurtserver, and W. S. Warren, Opt. Lett. **32**, 2641 (2007).
5. T. Ye, D. Fu, and W. S. Warren, Photochem. Photobiol. **85**, 631 (2009).
6. D. Fu, T. Ye, T. E. Matthews, J. Grichnik, L. Hong, J. D. Simon, and W. S. Warren, J. Biomed. Opt. **13**, 054036 (2008).
7. T. E. Matthews, I. R. Piletic, M. A. Selim, M. J. Simpson, and W. S. Warren, Sci. Transl. Med. **3**, 71ra15 (2011).
8. M. J. Simpson, K. E. Glass, J. W. Wilson, P. R. Wilby, J. D. Simon, and W. S. Warren, J. Phys. Chem. Lett. **4**, 1924 (2013).
9. T. E. Villafana, W. P. Brown, J. K. Delaney, M. Palmer, W. S. Warren, and M. C. Fischer, Proc. Natl. Acad. Sci. USA **111**, 1708 (2014).
10. J. Miyazaki, H. Tsurui, A. Hayashi-Takagi, H. Kasai, and T. Kobayashi, Opt. Express **22**, 9024 (2014).
11. V. N. Mahajan, J. Opt. Soc. Am. A **3**, 470 (1986).
12. S. W. Hell, P. E. Hanninen, A. Kuusisto, M. Schrader, and E. Soini, Opt. Commun. **117**, 20 (1995).
13. M. O. Cambaliza and C. Saloma, Opt. Commun. **184**, 25 (2000).
14. P. P. Mondal and A. Diaspro, Opt. Commun. **281**, 1855 (2008).
15. K. A. Serrels, E. Ramsay, and D. T. Reid, Appl. Phys. Lett. **94**, 073113 (2009).
16. E. J. Botcherby, R. Juškaitis, and T. Wilson, Opt. Commun. **268**, 253 (2006).
17. G. J. Brakenhoff, P. Blom, and P. Barends, J. Microsc. **117**, 219 (1979).
18. B. Sick, B. Hecht, and L. Novotny, Phys. Rev. Lett. **85**, 4482 (2000).
19. S. B. Ippolito, P. Song, D. L. Miles, and J. D. Sylvestri, Appl. Phys. Lett. **92**, 101109 (2008).
20. K. Kitamura, K. Sakai, and S. Noda, Opt. Express **18**, 4518 (2010).
21. S. B. Purnapatra, S. Bera, and P. P. Mondal, Sci. Rep. **2**, 692 (2012).
22. A. Avramescu, T. Lermer, J. Müller, C. Eichler, G. Bruederl, M. Sabathil, S. Lutgen, and U. Strauss, Appl. Phys. Express **3**, 061003 (2010).
23. J. Kasai, R. Akimoto, T. Hasama, H. Ishikawa, S. Fujisaki, S. Tanaka, and S. Tsuji, Appl. Phys. Express **4**, 082102 (2011).
24. M. Selmke and F. Cichos, Phys. Rev. Lett. **110**, 103901 (2013).
25. P. Dufour, M. Piche, Y. De Koninck, and N. McCarthy, Appl. Opt. **45**, 9246 (2006).